

# Surface and Corner Multifractality at the Metal-Insulator Transition in the Two-Dimensional Spin-Orbit (Symplectic) Symmetry Class

H. O. Buse,<sup>1</sup> A. R. Subramaniam,<sup>2,3</sup> A. Furusaki,<sup>1</sup> I. A. Gruzberg,<sup>2,3</sup> and A. W. W. Ludwig<sup>3,4</sup>

<sup>1</sup>Condensed Matter Theory Laboratory, RIKEN, Wako, Saitama 351-0198, Japan

<sup>2</sup>James Franck Institute, University of Chicago, 5640 South Ellis Avenue, Chicago, Illinois 60637, USA

<sup>3</sup>Kavli Institute for Theoretical Physics, University of California, Santa Barbara, California 93106, USA

<sup>4</sup>Physics Department, University of California, Santa Barbara, California 93106, USA

(Dated: September 6, 2006)

We study the multifractality of critical wave functions at boundaries and corners at the metal-insulator transition (MIT) for noninteracting electrons in the two-dimensional (2D) spin-orbit (symplectic) universality class. Multifractal exponents for wave function moments near a boundary are found to be different from those in the bulk. Multifractal exponents at a corner are found to be directly related to those at a straight boundary through a relation arising from conformal invariance. This provides direct numerical evidence for conformal invariance at the 2D spin-orbit MIT.

PACS numbers: 73.20.Fz, 72.15.Rn, 05.45.Df

Anderson metal-insulator transitions (MITs), i.e., localization-delocalization transitions of noninteracting electrons, are continuous phase transitions driven by disorder. At the transition, wave functions (WFs) are neither localized nor simply extended, but are complicated scale invariant fractals exhibiting multifractal behavior characterized by a continuous set of scaling exponents [1, 2, 3, 4]. In a recent Letter Subramaniam et al. [5] extended the notion of multifractality (MF) to the boundaries of the sample ("surface MF"), and showed that near boundaries critical WFs are characterized by multifractal exponents that are different from those in the bulk. These issues were illustrated with a few explicit examples. In this Letter we study surface MF at the two-dimensional (2D) MIT for non-interacting electrons with spin-orbit scattering (symplectic universality class) [6], and extend the surface MF analysis to boundaries with corners ("corner MF").

In two dimensions the universal critical properties at a host of conventional phase transitions are known to be described by conformal field theories (CFTs) [7]. It is natural to expect that disorder-averaged observables at a localization-delocalization transition in 2D are also governed by a (non-unitary) CFT. If so, then conformal symmetry is expected to impose severe constraints on disorder averaged local quantities, including moments of WF amplitudes. In particular, this would lead (following [8]), as we show, to a simple exact prediction relating corner and surface multifractal exponents. Here, we show numerically that at the 2D spin-orbit MIT this prediction is indeed valid for sufficiently low moments of WF amplitudes. We thereby provide direct numerical evidence for the presence of conformal symmetry at this 2D MIT. (For higher moments the disorder average is dominated by contributions from rare events [9], which makes it difficult to verify the prediction numerically.)

We begin by introducing corner and surface MF [5, 10] for a rhombus [Fig. 1 (a)] and a cylinder [Fig. 1 (b)], both

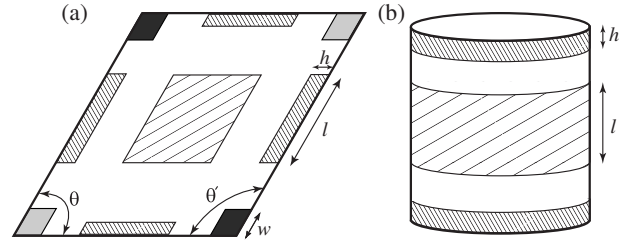


FIG. 1: Systems studied: (a) A rhombus with the bulk, surface and corner regions of sizes  $l$ ,  $l$ ,  $h$ , and  $w$  sites, correspondingly; (b) A cylinder with the bulk ( $L$ ,  $l$ ) and surface ( $L$ ,  $h$ ) regions.

having edges of length  $L$ . All WFs  $\psi(r)$  vanish at the boundaries. We define the corner ( $c$ ) with opening angle  $\theta$ , surface ( $s$ ), and bulk ( $b$ ) regions of the rhombus, and similar regions  $s, b$  of the cylinder, as illustrated in Fig. 1. In each region  $c, s$ , or  $b$ , the MF of WFs is characterized by the scaling of the  $q$ -th moment of  $j(\mathbf{r})^2$  with the system size  $L$  (all WFs  $\psi(r)$  are normalized),

$$L^{d_x} \overline{j(\mathbf{r})^2}^q \sim L^{-\frac{x}{q}}; \quad (x = c; s; b); \quad (1)$$

where  $d_x$  is the spatial dimension of each region ( $d_b = 2$ ,  $d_s = 1$ , and  $d_c = 0$ ). The overbar represents the ensemble (disorder) average and the simultaneous spatial average over a region  $x$  surrounding the point  $r$ .  $\frac{b}{q}$ ,  $\frac{s}{q}$ , and  $\frac{c}{q}$  are the bulk, surface, and corner multifractal exponents, respectively. Nonvanishing anomalous dimensions  $\frac{x}{q}$ ,

$$\frac{x}{q} = \frac{x}{q} - 2q + d_x; \quad (2)$$

distinguish a critical point from a simple metallic phase in which  $\frac{x}{q} = 0$ . By the definition (1, 2),  $\frac{x}{q}$  vanish at  $q = 0$  and  $1$ . The so-called parabolic approximation for MF amounts to assuming that  $\frac{x}{q} = [q(1 - q)]$  is independent of  $q$ . The exponent defined in Ref. [5] is absent in Eq. (2) because the local density of states is independent of energy at the spin-orbit MIT.

The multifractal singularity spectra  $f^*(\alpha)$  are obtained from  $\chi_q$  through Legendre transformation,

$$f^*(\alpha) = \alpha \chi_q - \chi_q; \quad \alpha = \frac{d\chi_q}{d\log L}; \quad (3)$$

$f^*(\alpha)$  have the meaning of fractal dimensions: the number of points  $r \leq x$ , where  $j(r)^2$  scales as  $L^\alpha$ , is proportional to  $L^{f^*(\alpha)}$ . This gives a direct relation between  $f^*(\alpha)$  and the probability distribution functions of WF amplitudes:

$$P_x(j^2) = j^2 L^{f^*(\alpha)} d\alpha; \quad \alpha = \frac{\ln j^2}{\ln L}; \quad (4)$$

Since  $f^*(\alpha) \leq d = 0$ , the ensemble average is essential for defining corner MF  $\chi_q$ .

Suppose that the  $q$ -th moment  $j(r)^{2q}$  is represented by a local operator in an underlying critical field theory describing disorder averages. The scaling dimension of this operator will then equal  $-\chi_q$  [11]. If the field theory possesses conformal invariance and if the operator is (Virasoro) primary, then the relation  $\chi_q = -\frac{s}{q}$  between the surface and corner exponents can be derived [8] from the conformal mapping  $w = z^s$ . This yields

$$\chi_q = 2 - (\frac{s}{q} - 2); \quad f^*(\alpha) = -f^s(\frac{s}{q} - 1); \quad (5)$$

The validity of these relations provides direct evidence for conformal invariance at a 2D localization-delocalization critical point. We note, however, that Eqs. (5) are valid only if  $\chi_q > 0$ , because  $\alpha$  is a positive-definite variable for normalized WFs [see Eq. (4)]. It is expected [9] that for  $q > q^*$  (where  $q^*$  is a solution to  $\chi_q = 0$ ) the exponents  $\chi_q$  become independent of  $q$ , while  $\chi_{q^*} = 0$  [Eq. (3)]. With the definition (2) this leads to a modified relation between  $\chi_q$  and  $\chi_{q^*}$ :

$$\chi_q = \begin{cases} \frac{8}{q} - \frac{s}{q}; & q < q^* \\ -\frac{s}{q} - 2(q - q^*); & q > q^* \end{cases} \quad (6)$$

In a recent paper Merlin et al. [12] pointed out that  $\chi_q^b$  obey the relation  $\chi_q^b = \frac{1}{q} \chi_q$ , which is expected to hold also for surface MF. In two dimensions this leads to

$$f^*(\frac{s}{1-q}) = \frac{\frac{s}{1-q}}{2} = f^*(\frac{s}{q}) - \frac{s}{2}; \quad \frac{s}{1-q} = 4 - \frac{s}{q}; \quad (7)$$

We show numerically that in the bulk,  $\chi_q^b$  and  $f^b(\frac{s}{q})$  indeed satisfy these relations at the 2D spin-orbit MIT. For surface MF ( $\alpha = s$ ), larger-scale numerical calculations than ours are required to confirm these relations.

To test these theoretical proposals for the 2D spin-orbit MIT, we employ the "SU(2) model" defined in Ref. [13], which is a tight-binding model on a 2D square lattice with on-site disorder and a random SU(2) nearest-neighbor

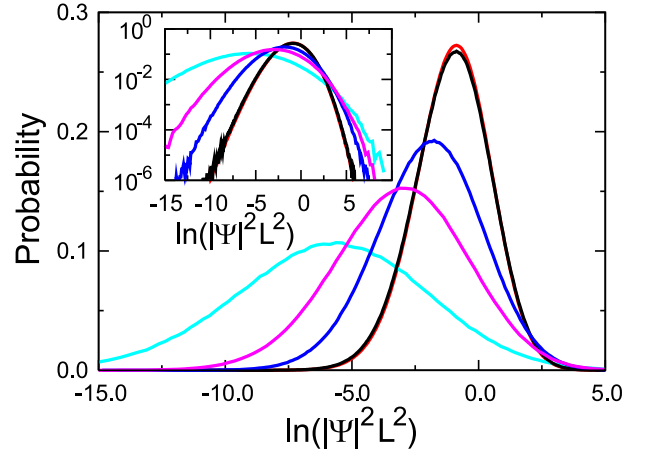


FIG. 2: Distribution functions of logarithm of probability amplitudes  $\ln(j^2 L^2)$  on tori (red), in the bulk region of cylinders (black), in the surface region of cylinders (blue), and in the corner region with  $s=2$  (pink) and  $s=4$  (cyan);  $L=120$ . Inset: Semi-logarithmic plot.

hopping. We consider four different lattice geometries:

- (i) torus, i.e., a square lattice with periodic boundary conditions (PBC) imposed in the  $x$  and  $y$  directions,
- (ii) cylinder [Fig. 1(b)] with PBC imposed in the  $x$  direction and open boundary conditions (OBC) in the  $y$  direction,
- (iii) square with OBC in the  $x$  and  $y$  directions, and
- (iv) rhombus [Fig. 1(a)] with  $s=4$  and  $s^0 = 3=4$  and OBC imposed in the  $x$  and  $y$  directions. In all these geometries the number of lattice sites is  $L^2$ .

For the scaling analysis the system size  $L$  is varied through  $L = 24, 30, 36, 48, 60, 72, 96$ , and  $120$ . For a fixed on-site disorder strength  $W_c$ , we examined  $6 \times 10^4$  samples with different disorder configurations for each  $L$ . We have used the forced oscillator method [14] to diagonalize the Hamiltonian, and extracted one critical WF from each sample which had the energy eigenvalue closest to the critical energy  $E_c = 1$  at  $W_c = 5.952$  (in the unit of hopping strength). For the results presented below, we have set  $l = L/6$ ,  $h = 1$  for the cylinders [Fig. 1(b)], and  $w = 4$  for the corners [Fig. 1(a)]. We have numerically confirmed that the exponents computed in the bulk regions of rhombi and cylinders agree with those of tori within statistical error bars. Also, the multifractal exponents for the surface region of rhombi are, within error bars, equal to those computed for the surface region of cylinders. In the following figures the bulk (surface) exponents are those computed for tori (for the surface region of cylinders).

Figure 2 shows the probability distribution functions of  $\ln(j(r)^2)$  measured for  $r$  at corners with angle  $s=4$  (cyan) and  $s=2$  (pink), at the boundary of cylinders (blue), and in the bulk region of cylinders (black) at the fixed system size  $L=120$ . Each distribution function is normalized in the region where it is defined. The distribution function calculated for tori is also shown in red as a reference, which agrees quantitatively with the

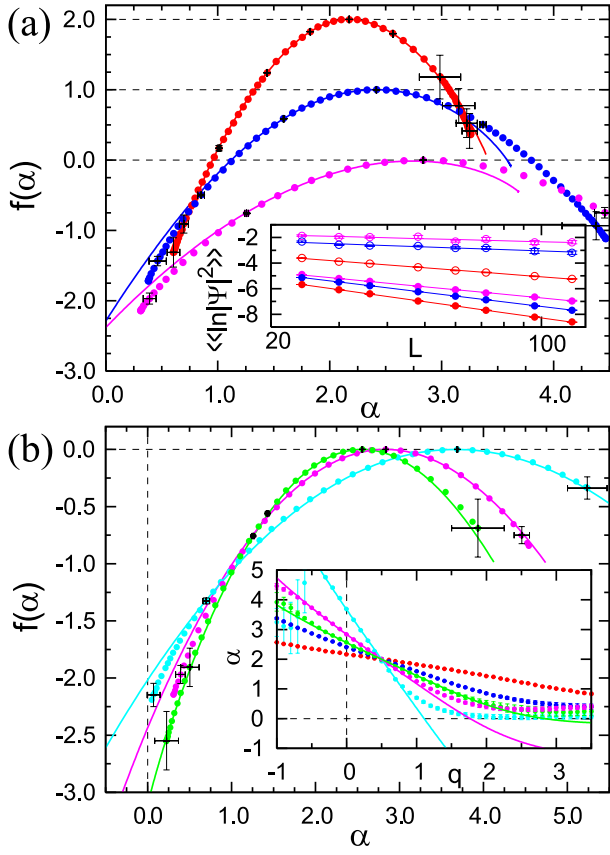


FIG. 3: (a) Bulk (red), surface (blue), and corner ( $\alpha = 2$ ) (pink)  $f(\alpha)$  spectra, with error bars shown at integer values of  $q$ . Thin red, blue, and pink lines represent  $f^x(\alpha) + 2$ . Inset: Scaling plot of Eq. (8) at  $q = 1$  (filled circles) and  $q = 3$  (open circles). (b) Corner  $f(\alpha)$  spectra at  $\alpha = 4$  (cyan),  $\alpha = 2$  (pink), and  $\alpha = 3 = 4$  (green), with error bars shown at integer  $q$  (and at  $q = 0.5$  for  $\alpha = 4$ ). Thin lines represent the conformal relation, Eqs. (5). Inset: Numerical results of  $x_q$  compared with Eqs. (5) (colored thin lines).

bulk distribution function (black), as expected. Clearly, the distribution functions for bulk, surface, and corner with  $\alpha = 2$  and  $\alpha = 4$ , are all different, and, in this order, the peak position is shifted to the left, in agreement with the expectation that WF amplitudes should be smaller near edges. In the same order, the distributions become broader with longer (presumably power-law) tails at  $j \propto L^2$ . This means that for large  $q$  the moments  $j(r) \propto j^q$  can become larger near edges (corners) than in the bulk, as the higher moments are dominated by long tails [9].

We calculate  $x_q$  and  $f^x(x_q)$  using [see (1, 3)]

$$\ln \ln j \propto \frac{\overline{j(r)^q \ln j(r)^q}}{\overline{j(r)^q}} \propto x_q \ln L; \quad (8)$$

$$\ln j(r)^q \propto f^x(x_q) \propto x_q \ln L; \quad (9)$$

The inset of Fig. 3(a) shows  $\ln \ln j \propto j^q$  as functions of  $L$ , computed for tori ( $x=b$ ), at the boundary of cylinders ( $x=s$ ), and at the corners ( $\alpha = 2$ ) of squares. This

inset clearly exhibits distinct scaling behavior for bulk, surface, and corner regions for the displayed values of  $q = 1, 3$ .

Figure 3(a) shows  $f^x(\alpha)$  of the bulk, surface, and corner ( $\alpha = 2$ ) regions. Clearly, in this order, the spectra  $f^x(\alpha)$  are seen to become broader and their maxima  $\alpha_0$  are shifted to the right ( $\alpha_0 = 2.173 \pm 0.001$ ,  $\alpha_0 = 2.417 \pm 0.002$ ,  $\alpha_0 = 2.837 \pm 0.003$ ), in accordance with Fig. 2 and Eq. (4). (Recall that the maximal values of  $f^x(\alpha)$  are the spatial dimensions  $d_x$ .)

The data points of the bulk spectrum  $f^b(\alpha)$  [red dots in Fig. 3(a)] lie on top of the thin red line which represents data points [15] for  $f^b(\alpha)$  in Eq. (7). The relation (7) is thus confirmed numerically, and this indicates the accuracy of our  $f^b(\alpha)$  data. Incidentally, the value of the typical bulk exponent  $\alpha_0$  agrees with earlier calculations [16, 17] but not with Ref. [18]. Furthermore, our  $\alpha_0$  satisfies the relation  $(\alpha_0 - 2) = 1/\alpha_c$  [3], where  $\alpha_c = 1.843$  is the quasi-one-dimensional localization length at the MIT, normalized by the wire width, as obtained in [13]. The surface spectrum  $f^s(\alpha)$  (blue) is also seen to satisfy the relation (7) for  $1 \leq \alpha \leq 3$ , but there are discrepancies between the blue dots and the line  $f^s(\alpha)$  when  $\alpha > 3$  ( $q < 0.7$ ) and  $\alpha < 1$  ( $q > 2$ ); this might mean that our system size and our number of samples are not large enough for these larger values of  $j \propto \alpha$ .

Figure 3(b) shows the corner spectra  $f(\alpha)$  at  $\alpha = 3 = 4$  (green),  $\alpha = 2$  (pink), and  $\alpha = 4$  (cyan). As  $\alpha$  decreases, the peak position moves to the right ( $\alpha_0 = 2.558 \pm 0.003$ ,  $\alpha_0 = 2.837 \pm 0.003$ , and  $\alpha_0 = 3.689 \pm 0.006$ ) and the spectra become broader, indicating that at smaller

the typical value of a WF amplitude is smaller but its distribution is broader. The numerical data (dots) are compared with the predicted curves computed from Eq. (5) using  $f^s(\alpha)$  of Fig. 3(a). The agreement between the numerical data and the predicted curves is excellent, except for small deviations seen at  $\alpha = 1$ . The inset of Fig. 3(b) shows  $x_q$  as functions of  $q$  [Eq. (3)] where the thin lines represent  $x_q$  computed with  $\alpha_q$  as input in Eq. (5). We note that  $x = 2$  at  $q = 1/2$  as a consequence of the relation  $\alpha_q - 2 = (x_q - 2)$ , Eq. (7). We see that the numerical data for  $x_q$  must deviate from the predicted lines, Eq. (5), when  $x_q < 1$ , in order to satisfy the constraint  $x_q > 0$ . We expect that in the limit  $L \rightarrow \infty$ ,  $x_q$  be given by Eq. (5) for  $q < q_c$  and by  $x_q = 0$  for  $q > q_c$ . Numerical results for  $\alpha = 4$  and  $\alpha = 2$  indicate that for corners,  $x_q$  can exceed 4, in contrast to  $x < 4$  (valid in the bulk) [12]. It is worth noting that the numerical data of  $x_q$  used in the predicted curve (5) in Fig. 3(b) are mostly within the range  $1 \leq x \leq 3$ .

The anomalous dimensions  $x_q$  are computed from the scaling  $\overline{j(r)^q} \propto j(r)^{x_q} L^{x_q}$ , which follows from Eqs. (1) and (2). Figure 4(a) shows the bulk anomalous dimension  $x_q$  (red) and its mirror image across  $q = 1/2$

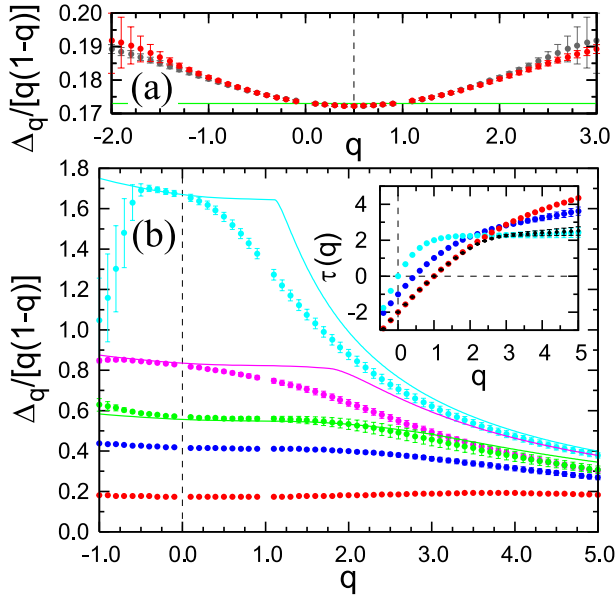


FIG. 4: (a) The numerical data for the rescaled bulk exponents  $b_q$  (red) are compared with their error margin  $b_{1-q}$  (grey). The green line represents  $b_0 = 2$ . (b) Rescaled exponents  $\Delta_q/[q(1-q)]$  for the bulk (red), the surface (blue), and corners with  $\epsilon=4$  (cyan),  $\epsilon=2$  (pink), and  $\epsilon=3=4$  (green). Thin lines represent the theoretical prediction, Eq. (6). Inset: Bulk (red), surface (blue), and corner ( $\epsilon=4$ , cyan) exponents  $x_q$ , and  $x_q$  of a whole rhombus with  $\epsilon=4$  (black) | see text.

line  $b_{1-q}$  (grey), both of which are rescaled by  $q(1-q)$ . Note that the rescaling magnifies small numerical errors around  $q=0$  and  $q=1$ . Nevertheless the numerical data satisfy the relation  $b_q = b_{1-q}$  of Ref. [12] for  $1 < q < 2$  where statistical errors are small. It is also clear from Fig. 4(a) that  $b_q/[q(1-q)]$  varies with  $q$ , which means that the bulk spectrum  $f^b(\cdot)$  is not exactly parabolic.

Figure 4(b) compares the anomalous dimensions  $x_q$  for bulk, surface, and corners with  $\epsilon=4$ ;  $\epsilon=2$ , and  $\epsilon=3=4$ . The corner dimensions  $x_q$  are not as symmetric about  $q=1/2$  as  $b_q$ . This reflects relatively poor statistics of the corner data as compared with the bulk data for larger values of  $q$ . The solid thin lines represent the theoretical prediction (6) from the conformal mapping. For sufficiently small values of  $q$  the numerical results of  $x_q$  are in good quantitative agreement with the prediction (6). This provides direct numerical evidence for the presence of conformal symmetry at the MIT in the 2D spin-orbit symmetry class. When  $q \approx 1$ , Fig. 4(b) shows discrepancies between the numerical results and the prediction from CFT, which are enhanced near  $q=1$  by the  $(1-q)^{-1}$  factor. But we emphasize that since  $f(\cdot) \geq 0$ , the average of  $\int (r) f^q$  is dominated by contributions from rare events, except very close to  $q=0$ . Therefore, reducing numerical uncertainties further would require computations on larger system sizes and averaging over much larger number of samples. Given these reasons for the discrepancies, we think that the data provide strong

evidence for the presence of conformal symmetry.

The inset of Fig. 4(b) shows the exponents  $x_q$  for bulk, surface, and corners. We see that  $x_q^{\epsilon=4}$  (cyan) is constant for  $q > q_{\epsilon=4} = 1$  reflecting the exchange between top and bottom lines in Eq. (6) which happens at  $x_q^{\epsilon=4} = 0$ . It appears that  $x_q^{\epsilon=4}$  becomes smaller than both  $x_q^s$  and  $x_q^b$  for  $q \approx 2.5$ , which is when the corner exponent  $x_q^{\epsilon=4}$  controls the MF of the whole sample with a  $\epsilon=4$  corner, as shown in black. In a sample without corners such as a cylinder, the surface exponent  $x_q^s$  controls the MF of the entire sample for sufficiently large  $q$ . This confirms and generalizes the observations made in Ref. [5]. We end by quoting results obtained for the bulk,  $D_1^b = 1.83 \pm 0.02$  and  $D_2^b = 1.64 \pm 0.01$ , and for the surface multifractal dimensions,  $D_1^s = 0.59 \pm 0.04$  and  $D_2^s = 0.20 \pm 0.12$ , where  $D_q^x = d_x + x_q/(q-1)$ .

In summary, we have numerically calculated bulk, surface, and corner multifractal exponents at the MIT in the 2D spin-orbit symmetry class. We have shown that the corner exponents  $x_q$  are related to the surface exponents  $x_q^s$  via the (modified) conformal relation (6) for sufficiently small  $q$ . This provides direct evidence for the presence of conformal symmetry at this critical point.

We thank A. Mirlin for discussions, and Kavli Institute for Theoretical Physics at UCSB where this paper was finished. This work was supported by the Next Generation Super Computing Project, Nanoscience Program, MEXT, Japan, the NSF under Grant No. PHY 99-07949, the NSF MRSEC Program under DMR-0213745, the NSF Career award DMR-0448820, the Alfred P. Sloan Foundation, and Research Corporation. Numerical calculations have been mainly performed on the RIKEN Super Combined Cluster System. | Note added: When we were finishing this article, we became aware of the recent numerical work on the bulk MF in the 2D symplectic class by Mildenberger and Evers [19]. Their results on bulk MF agree with ours.

- 
- [1] F. Wegner, Z. Phys. B 36, 209 (1980).
  - [2] C. Castellani and L. Peliti, J. Phys. A 19, L429 (1986).
  - [3] M. Janssen, Int. J. Mod. Phys. B 8, 943 (1994); Phys. Rep. 295, 1 (1998).
  - [4] A. D. Mirlin, Phys. Rep. 326, 259 (2000).
  - [5] A. R. Subramaniam et al., Phys. Rev. Lett. 96, 126802 (2006).
  - [6] S. Hikami, A. I. Larkin, and Y. Nagaoka, Prog. Theor. Phys. 63, 707 (1980).
  - [7] A. A. Belavin, A. M. Polyakov, and A. B. Zamolodchikov, Nucl. Phys. B 241, 333 (1984).
  - [8] J. L. Cardy, Nucl. Phys. B 240, 514 (1984).
  - [9] F. Evers and A. D. Mirlin, Phys. Rev. Lett. 84, 3690 (2000); A. D. Mirlin and F. Evers, Phys. Rev. B 62, 7920 (2000).
  - [10] A. R. Subramaniam et al., unpublished.
  - [11] B. Duplantier and A. W. W. Ludwig, Phys. Rev. Lett. 66, 247 (1991).
  - [12] A. D. Mirlin et al., Phys. Rev. Lett. 97, 046803 (2006).

- [13] Y. Asada, K. Slevin, and T. Ohtsuki, Phys. Rev. Lett. 89, 256601 (2002); Phys. Rev. B 70, 035115 (2004).
- [14] T. Nakayama and K. Yakubo, Phys. Rep. 349, 239 (2001).
- [15] The data points are drawn very closely spaced so as to appear to the eye as a continuous curve.
- [16] L. Schweitzer, J. Phys. Condens. Matter 7, L281 (1995).
- [17] R. Merkt, M. Janssen, and B. Huckestein, Phys. Rev. B 58, 4394 (1998).
- [18] P. Markos and L. Schweitzer, J. Phys. A 39, 3221 (2006).
- [19] A. Mildenberger and F. Evers, cond-mat/0608560.